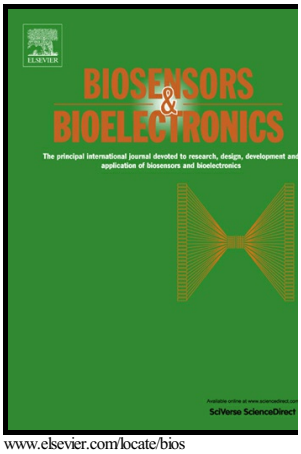

A microarray platform for detecting disease-specific circulating miRNA in Human serum

Somenath Roy, Jun Hui Soh, Jackie Y. Ying

www.elsevier.com/locate/bios

PII: S0956-5663(15)30362-6
DOI: http://dx.doi.org/10.1016/j.bios.2015.08.039
Reference: BIOS7935

To appear in: *Biosensors and Bioelectronic*

Received date: 23 June 2015
Revised date: 17 August 2015
Accepted date: 18 August 2015

Cite this article as: Somenath Roy, Jun Hui Soh and Jackie Y. Ying, A microarray platform for detecting disease-specific circulating miRNA in Human serum, *Biosensors and Bioelectronic* http://dx.doi.org/10.1016/j.bios.2015.08.039

A microarray platform for detecting disease-specific circulating miRNA in human serum

Somenath Roy[1], Jun Hui Soh, Jackie Y. Ying*

Institute of Bioengineering and Nanotechnology, 31 Biopolis Way, The Nanos, Singapore 138669, Singapore

Abstract

Circulating microRNAs (miRNAs) are emerging as potential blood-based biomarkers for cancer and other critical diseases. To profile the expression levels of these tiny molecules, especially in a point-of-care setting, it is imperative to quantify them directly in complex biological fluids. Herein, we report on the development of a microarray platform with carboxyl-polyethylene glycol (PEG) as a functional layer and aminated hairpin nucleic acid molecules as target-specific capture probes (CPs). Due to the anti-fouling effect conferred by the carboxyl-PEG layer, we could directly detect as little as 10 fM of miRNA targets in 20 µl of unprocessed human serum. In contrast to the conventional miRNA microarrays, our platform does not require RNA extraction, labeling and target amplification, thus significantly reducing both the sample preparation steps as well as the total assay duration. The use of specially designed hairpin CPs entails reliable discrimination of miRNA sequences with high sequence homology. A nanoparticle-based detection technique, with the help of differential interference contrast (DIC) microscopy, offers excellent resolution down to a single molecule. With the capability of detecting disease-specific miRNA targets directly in human serum, our microarray platform has potential applications in rapid, minimally invasive clinical diagnostic assays.

Keywords: Biosensor, Circulating microRNA, Microarray, Hairpin probes, DIC microscopy, Gold nanoparticles

---

[1] Present address: Sensor and Actuator Division, CSIR-Central Glass and Ceramic Research Institute, 196 Raja S. C. Mullick Road, Kolkata 700032, India

* Corresponding author. Fax: +65 6478-9080.

E-mail address: jyying@ibn.a-star.edu.sg (J. Y. Ying).

1. Introduction

MicroRNAs (miRNAs) are a class of short (18–24 nucleotides) non-coding RNA molecules that negatively regulate gene expression at the post-transcriptional level (Ambros, 2004; Bartel, 2004). They play important roles in a variety of physiological and pathological processes, such as development, differentiation, cell proliferation, apoptosis, and stress responses (Kloosterman and Plasterk, 2006; Stefani and Slack, 2008). Though miRNAs have originally emerged as cell-based biomarkers, recent reports indicated that they exist in cell-free form as well (Chim et al., 2008; Gilad et al., 2008). In fact, extracellular miRNAs have been detected in multiple body fluids including plasma, serum, saliva, and urine (Hanke et al., 2010; Weber et al., 2010). Aberrant expression levels of such circulating miRNAs have been associated with cancer (Calin and Croce, 2006; Esquela-Kerscher and Slack, 2006; Zhao et al., 2010), cardiovascular disorders (Corsten et al., 2010), abnormal pregnancies (Zhang et al., 2009), diabetes (Zampetaki et al., 2010), autoimmune diseases (Wang et al., 2010), and so on. Given the facts that circulating miRNAs are highly stable (Chen et al., 2008), e.g. resistant to RNase digestion, and that their expression levels are reproducibly consistent among individuals of the same species, they show promises as novel and non-invasive biomarkers for disease detection.

With the emergence of miRNAs as key players in disease diagnosis and screening, development of rapid, sensitive, and quantitative miRNA detection is of high interest. Chip-based devices have been used for the ultra-trace detection of analytes (Hou et al., 2014; Hou et al., 2015), and the development of a nucleic acid-based microarray is particularly useful for high-throughput detection and profiling of miRNA targets. The small size of miRNAs, however, poses a major challenge toward developing a reliable assay. For a short target-probe hybrid, the oligonucleotide annealing temperature is low, thereby lessening the stringency of hybridization and greatly increasing the risk of false-positive signals. Selective detection of miRNA is further challenged due to high sequence homology among family members, which is as close as a single base variation (www.mirbase.org). Based on thermodynamic analysis, a structurally constrained probe should increase specificity of target recognition as compared with a linear DNA probe (Bonnet et al., 1999). In fact, stem-loop (hairpin) oligomer probes have been shown to recognize single-nucleotide polymorphism (SNP) in DNA targets (Tyagi et al., 1998). To

handle the challenge of discriminating high sequence homology in miRNA, we have fabricated a microarray of hairpin capture probes (CPs), the loop of which is complementary to the target (Fig. 1). In a sample solution, if the target miRNA is present, the hairpin opens up and part of it makes a duplex with the specific miRNA. A gold nanoparticle-tagged signaling probe (SP) then marks the probe-target hybrid. The nanoparticles are then imaged by differential interference contrast (DIC) microscopy, which offers single-molecule resolution (Roy et al., 2011). The nanoparticle-based imaging technique further relieves the microarray from limitations, such as photobleaching and spectral cross-talk, associated with conventional fluorescent microarrays (Lewis et al., 2005; Roy et al., 2009).

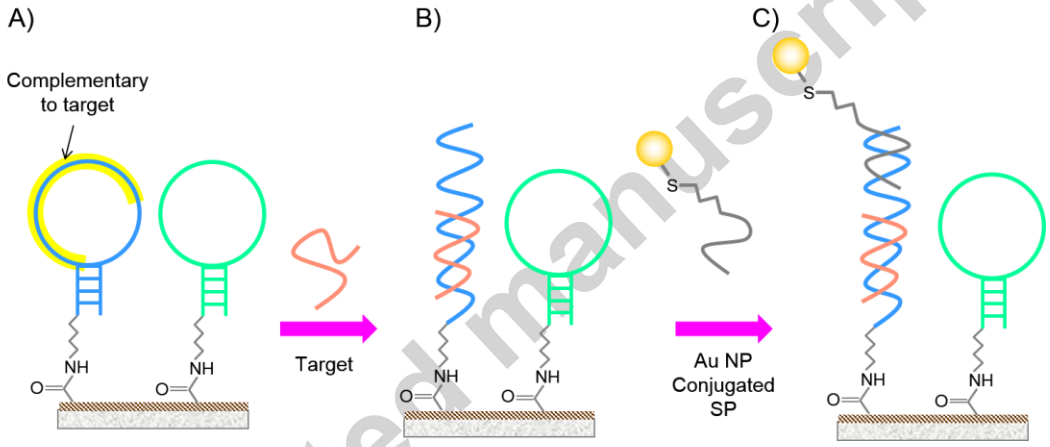

Fig. 1. Schematic illustration of the miRNA detection assay on a microarray, which is produced on a carboxyl-PEG functionalized glass slide. (A) Immobilization of hairpin CPs. (B) CP–target hybridization at the loop region. (C) CP–SP hybridization at the stem region.

In addition to sensitivity issues, the performance of a microarray would be affected by non-specific adsorption. For point-of-care (POC) applications, it is desirable that the end result is obtained without extensive sample preparation (e.g. RNA isolation, PCR amplification, and tagging). Furthermore, sample collection should preferably be minimally invasive (unlike tissue biopsies). In this respect, human serum is a favorable matrix (De et al., 2009), in which at least ¼ of the circulating miRNA in blood is still preserved (Heneghan et al., 2010). Moreover, serum is relatively easy to handle in a

microarray format than whole blood. However, serum consists of over 20,000 proteins and various nucleic acids, making selective and sensitive detection of miRNA difficult due to interference, non-specific binding and biofouling from these biomolecules (Stern et al., 2010). We have developed specific surface functionalization schemes to produce a carboxyl-polyethylene glycol layer for minimal non-specific adsorption of proteins and nucleic acids, simultaneously ensuring efficient immobilization of hairpin CPs. In this paper, we demonstrated a highly sensitive and selective microarray platform, with designer hairpin CPs on a surface-functionalized layer, for the direct detection of target miRNAs from unprocessed human serum.

2. Material and methods

2.1. Materials and apparatus

Plain microscope glass slides purchased from VWR International (West Chester, PA), with dimensions of 25 mm × 75 mm × 1 mm were used for surface functionalization and fabrication of microarrays. Synthetic miRNA targets, aminated oligonucleotide CPs, and thiolated oligonucleotide SPs (Table 1) were custom-made by Sigma-Aldrich (Singapore). 3-aminopropyl triethoxysilane (APTES), N-ethyl-N'-(3-dimethylaminopropyl) carbodiimide (EDC), N-hydroxysulfosuccinimide sodium salt (sulfo-NHS), Zonyl® FSN fluorosurfactant, 5 M sodium cyanoborohydride ($NaBH_3CN$) solution and sterile-filtered human serum were purchased from Sigma-Aldrich (St. Louis, MO). Human serum was obtained from healthy human male AB plasma in the USA, sterile-filtered by the manufacturer, and used in this study without further processing. Glutaraldehyde (25%) and toluidine Blue O (TBO) dye were purchased from Merck KGaA (Darmstadt, Germany). Amino PEG acid, $COOH\text{-}(C_2H_4O)_{24}\text{-}C_2H_4\text{-}NH_2$ (MW = 1 kDa) was purchased from Nanocs Inc. (New York, NY). 5-nm Au nanoparticles (NPs) were obtained from BB International (Cardiff, UK). Dithiothreitol (DTT) was purchased from Gold Biotechnology, Inc.® (St. Louis, MO). All solutions were prepared with nuclease-free water, 20× saline sodium citrate (SSC) and 1× phosphate buffer saline (PBS), purchased from 1st Base Pte. Ltd. (Singapore).

The glass slides were treated with oxygen plasma using a CD300 gas plasma system from Europlasma NV (Oudenaarde, Belgium). Thermal curing of the glass slides

was conducted in a RTP-6 infrared lamp heating system from Ulvac-Riko, Inc. (Methuen, MA). Microarrays were printed on functionalized glass slides using the SpotBot® 3 Personal Microarrayers (Sunnyvale, CA).

Table 1. Sequence information of the oligonucleotides used in this study. Bolded sequences are complementary to their respective target miRNAs, and sequences in *italics* are complementary to the Au NP- or Cy3-conjugated SPs.

Annotation	Sequence
Hairpin (HPN) CP for miR-208b	5'–NH_2-$(CH_2)_6$-TTT TTC CGC GC**A CAA ACC TTT TGT TCG TCT TAT** TTA ATA TA*T GCG CGG GCG*–3'
hsa-miR-208b	5'–AUA AGA CGA ACA AAA GGU UUG U–3'
HPN CP for miR-335	5'–NH_2-$(CH_2)_6$-TTT TTC CGC GC**A CAT TTT TCG TTA TTG CTC TTG A**TT AAT ATA *TGC GCG GGC G*–3'
hsa-miR-335	5'–UCA AGA GCA AUA ACG AAA AAU GU–3'
SP HPN–thiol	5'–RS-S-$(CH_2)_6$-TTT TTT CGC CCG CGC A–3'
SP HPN–Cy3	5'–Cy3-TTT TTT CGC CCG CGC A–3'
HPN CP for *let-7a*	5'–NH_2-$(CH_2)_6$-TTT TTC CGC GC**A ACT ATA CAA CCT ACT ACC TCA** TTA ATA TA*T GCG CGG GCG*–3'
Linear CP for *let-7a*	5'– NH_2-$(CH_2)_6$-TTT TTT **AAC TAT ACA ACC**–3'
hsa-let-7a	5'–*UGA GGU AGU A*GG UUG UAU AGU U–3'
hsa-let-7b	5'–*UGA GGU AGU A*GG UUG UGU GGU U–3'
hsa-let-7f	5'–*UGA GGU AGU A*GA UUG UAU AGU U–3'
hsa-let-7g	5'–*UGA GGU AGU A*GU UUG UAC AGU U–3'
SP linear *let-7a*–thiol	5'–TAC TAC CTC ATT TTT T-$(CH_2)_3$-S-SR–3'

2.2. Functionalization of glass slide

The procedure for functionalizing glass slides is outlined in Fig. 2. Before functionalization, the glass slides were cleaned in Piranha solution (H_2SO_4:H_2O_2 = 3:1) at 120°C for 2 h. Caution: Piranha solution is highly oxidizing, corrosive, reactive and potentially explosive, therefore, appropriate personal protective equipment (i.e. neoprene

apron and face shield) should be worn at all times when handling it. Following Piranha treatment, the glass slides were rinsed thoroughly with deionized (DI) water and dried in nitrogen gas. The glass slides were then treated with oxygen plasma at 200 W for 10 min.

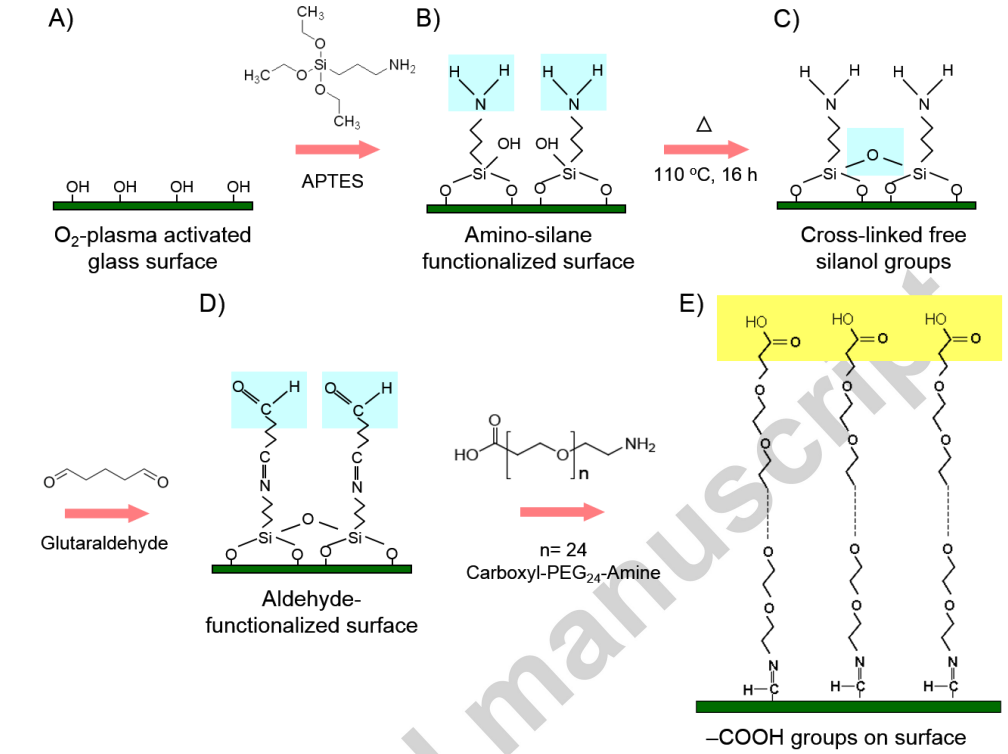

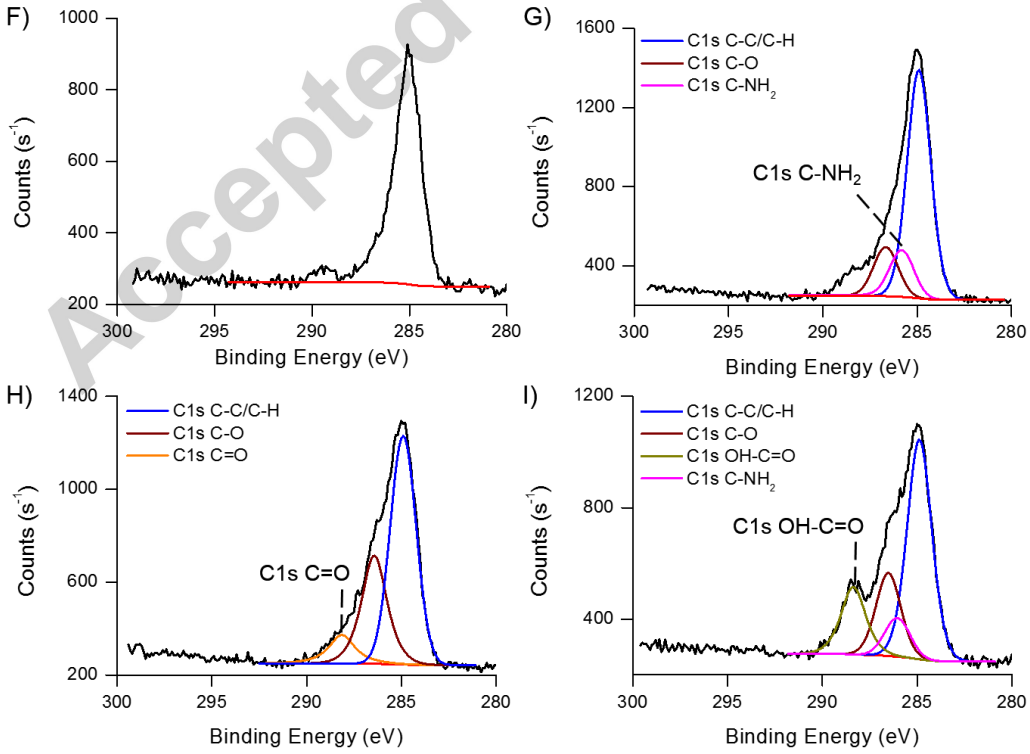

Fig. 2. (A–E) Schematic illustration of the procedure for surface functionalization of glass slides. (F–I) XPS C1s spectra of the surface functional groups on the glass slides after (F) washing with Piranha solution, (G) APTES coating, (H) glutaraldehyde coating, and (I) carboxyl-PEG functionalization.

Subsequently, to introduce primary amine groups on the surface, the glass slides were immersed in 5% (v/v) APTES (in ethanol) solution for 2 h at room temperature with gentle shaking. They were then rinsed thoroughly with pure ethanol and dried with nitrogen. Next, the glass slides were thermally cured at 110°C for 16 h. For the addition of surface aldehyde groups, the glass slides were immersed in 4% glutaraldehyde (diluted in 1× PBS) solution containing 50 mM $NaBH_3CN$ at room temperature for 2 h with gentle shaking. The slides were cleaned with 1× PBS and dried with nitrogen. Finally, to introduce a PEG layer containing surface carboxyl groups, the glass slides were immersed in 500 mM of amino-PEG-carboxylic acid (dissolved in 1× PBS) solution containing 50 mM $NaBH_3CN$ at room temperature overnight with gentle shaking. After treatment with carboxyl-PEG solution, the slides were washed with 1× PBS, and dried with nitrogen.

2.3. Quantification of surface carboxyl groups

Surface density of carboxyl groups on the glass slides was determined through evaluating the staining of basic TBO, following published procedure (Sano et al., 1993). TBO is a cationic blue dye derivative of phenothiazine ($C_{12}H_9NS$) (Tiraferri and Elimelech, 2012), which binds electrostatically to the negatively charged carboxyl group on the surface of the glass slides. The glass slides were immersed in 0.5 mM TBO solution (pH 10, adjusted with NaOH). Complexation between TBO and the carboxyl groups was conducted at room temperature for 5 h with mild shaking. During complexation, a calibration curve was constructed, where the absorbance of TBO solutions (in 50% acetic acid) at varying concentrations were measured. Absorbance values were measured using the Infinite® M200 microplate reader (Tecan Group Ltd.).

The maximum absorbance of the TBO molecules was determined to be 633 nm, and all absorbance values were taken at 633 nm.

After complexation, the glass slides appeared bluish due to staining by the TBO molecules. Subsequently, non-complexed TBO molecules were removed by washing the glass slides 3 times (5 min each) with 0.1 mM NaOH. Finally, the glass slides were immersed in 50% acetic acid solution for desorption of complexed TBO molecules. The desorption process was conducted at room temperature for 2 h with moderate shaking to ensure all bound TBO molecules were desorbed from the surface. Aliquots of the desorption solution were collected, and their absorbance values were measured and compared to the calibration curve to determine the surface carboxyl density. A 1:1 complexation ratio between TBO and carboxyl groups was assumed in the calculation of surface carboxyl density. The quantification process was repeated for a total of 3 glass slides.

2.4. Immobilizing CPs on functionalized glass slide for microarray production

In order to facilitate reaction between primary amine and carboxyl groups for the immobilization of aminated CPs, the glass slides were immersed in a solution containing 5 mM EDC and 10 mM sulfo-NHS (in 0.1 M 2-(N-morpholino)ethanesulfonic acid (MES) buffer, pH 5). This activated the surface carboxyl groups for the spontaneous reaction with primary amines, as EDC and sulfo-NHS would react with the carboxyl groups to form amine-reactive sulfo-NHS esters. The activation reaction was conducted at room temperature for 6 h with gentle shaking. Next, the glass slides were briefly washed with nuclease-free water and dried with nitrogen. 10 μM of aminated hairpin or linear CPs was then dissolved in 5× SSC (pH 7), and spotted in a microarray format using the SpotBot 3 microarrayer. Immobilization of the CPs was performed at room temperature overnight. Subsequently, the glass slides were washed in 5× SSC buffer, and then briefly in nuclease-free water to remove unbound CPs.

2.5. SP–Au NP conjugation

Conjugation of the single-stranded thiolated SP to Au NP was conducted following a published procedure (Zu and Gao, 2009). Briefly, 100 μM thiolated SPs were

treated with 0.1 M DTT (dissolved in nuclease-free water) at room temperature for 2 h, and then purified using a NAP-5 column (GE Healthcare). Stock Au NP solution was first incubated with 0.05% FSN for 15 min at room temperature. Next, NaCl solution was added to achieve a final concentration of 1 M. The solution retained its red color as the non-ionic FSN was able to stabilize the Au NPs against aggregation induced by the addition of salt (NaCl). 2 μM thiolated SPs were then added, and the conjugation reaction was conducted at room temperature for 2 h. Thereafter, non-conjugated thiolated SPs were removed by centrifugation at 16,000 *g* for 15 min. The SP–Au NP conjugates were resuspended in 0.1 M of PBS (pH 7). This process was repeated 3–5 times for complete removal of non-conjugated thiolated SPs.

2.6. Hybridization of target miRNA and SP on the microarray

miRNA targets of varying concentrations (1 fM–100 nM), dissolved either in 20 μl of 5× SSC buffer or in commercially obtained human serum, were applied to the immobilized CPs for CP–target hybridization. Hybridization was allowed to occur at room temperature over 4 h. The glass slides were then washed 3 times with 1× SSC buffer (1 min each) at 40°C, and with 5% ethanol (in nuclease-free water) for 30 s, with moderate shaking. After washing, the glass slides were dried with nitrogen.

Next, thiolated or Cy3-labeled SPs were added to the CP–target hybrid, and hybridization was allowed to occur at room temperature over 4 h. Lastly, the same washing steps were performed, except that they were conducted at room temperature.

2.7. Detection of miRNA targets using optical DIC imaging of Au NPs

miRNA targets were quantified through DIC imaging of Au NPs using an Olympus IX 81 microscope, which was equipped with Nomarski prisms and a computerized stage control. Visualization of the Au NPs was done under 60× magnification with 100 ms of exposure. Estimation of the surface coverage of Au NPs was conducted using the Metamorph® software (Molecular Devices, Inc., Sunnyvale, CA).

2.8. Detection of target sequence mismatch

Hairpin or linear CPs for the *hsa-let-7a* target (Table 1) were immobilized onto carboxyl-PEG functionalized glass slides following the procedures described earlier. Next, 100 nM of each of *hsa-let-7a*, *hsa-let-7b*, *hsa-let-7f* and *hsa-let-7g* targets (dissolved in 5× SSC buffer) was spotted onto a microarray with hairpin CPs, and on another microarray with linear CPs. Subsequent SP hybridization and DIC imaging steps were conducted as described earlier. The signal intensities for the above set of miRNAs with high sequence homology were analyzed to substantiate the efficacy of the hairpin CPs in discriminating sequence mismatch over their linear counterparts.

3. Results and discussion

3.1. Assay and mechanism for the detection of miRNA targets

Fig. 1 illustrates the principal steps for miRNA detection on our microarray. Specific CPs were spotted onto carboxyl-PEG functionalized glass slides by robotic spotting. Immobilization took place through covalent peptide bond formation between aminated CPs and activated carboxyl groups on the glass slide surface (Fig. 1A). The sequence complementary to the target miRNA was incorporated within the loop structure of the hairpin CP.

When the target was introduced, the hairpin structure would unfold and the complementary sequence in its loop region would form a duplex with the target miRNA (Fig. 1B). This unfolding would also expose the stem region, which contained base sequence complementary to the SP. Next, the Au NP-conjugated SPs were added, which would hybridize at the upper terminus of the already unfolded CPs (Fig. 1C). The Au NPs, which represented the target miRNA–probe duplexes, could be imaged under DIC microscopy. The surface coverage of Au NPs would directly correlate to the concentration of the target miRNAs in a given sample.

In the presence of a non-complementary (mismatched) target, the hairpin CP would retain its stem-loop structure as the mismatched target would not be able to change its conformation, and therefore would not hybridize. Without unfolding the CP, the Au NP-conjugated SP would not be able to bind to the stem region of the hairpin, thus

preventing false-positive signals (Fig. 1C). The use of a hairpin-structured CP in this study would therefore confer the detection assay with high target selectivity.

3.2. Functionalization of glass slides for anti-fouling effect

Fig. 2 illustrates the procedure of functionalizing glass slides with a carboxyl-PEG layer to achieve anti-fouling effect during detection of miRNA targets in biological fluids. Treating the glass slides with oxygen plasma (Fig. 2A) would activate silanol groups (SiOH) on the surface, promoting subsequent silanization reaction with APTES (Fig. 2B). Thermal curing of the glass slides at 110°C for 16 h (Fig. 2C) would result in the condensation of unreacted siloxane linkages, and produce a cross-linked monolayer of APTES on the surface. This crosslinking would reduce susceptibility of the APTES monolayer to hydrolysis (Halliwell and Cass, 2001). Schiff base formation between primary amine and aldehyde would take place in the next 2 functionalization steps involving glutaraldehyde (Fig. 2D) and carboxyl-PEG (Fig. 2E). Glutaraldehyde would act as an amine-reactive homo-bifunctional cross-linker for the covalent attachment of the carboxyl-PEG layer onto the glass slide surface. Schiff base would form readily at room temperature. However, it would be labile and unstable, unless it is reduced to secondary or tertiary amines, which are highly stable and would not hydrolyze in aqueous solutions by reducing agents such as sodium borohydride ($NaBH_4$) or $NaBH_3CN$. The latter is chosen because being a milder reducing agent, it would selectively reduce Schiff base only to a secondary amine, leaving reactive aldehyde groups at the opposite end of the glutaraldehyde free to react with the carboxyl-PEG.

Elemental surface characterization of the glass slides at each stage of functionalization was conducted using X-ray photoelectron spectroscopy (XPS). The area of analysis was 400 μm × 400 μm, and the depth of analysis was 5–10 nm. Fig. 2F shows the XPS C1s spectrum of a Piranha-cleaned plain glass slide without any functionalization. Addition of APTES and thermal curing yielded a XPS peak at 285.8 eV (Fig. 2G), which was attributed to the amino carbon atoms. Upon addition of glutaraldehyde, a peak emerged at 288.1 eV (Fig. 2H), which was attributed to the carbonyl carbon of aldehyde. After the addition of the carboxyl-PEG layer, a XPS peak appeared at 288.4 eV (Fig. 2I), which could be attributed to the carboxyl carbon.

The density and quality of surface carboxyl groups are vital for the dense immobilization of aminated CPs, and the sensitivity of miRNA targets detection. Also, signal intensity has been reported to be strongly dependent on the density of surface functional groups (Oh et al., 2005). Hence, quantifying the surface carboxyl groups was critical towards ensuring high assay quality. The TBO assay was utilized as it is an established dye adsorption method for surface carboxyl group quantification (Rodiger et al., 2011). The surface carboxyl density was determined by the TBO assay to be 1.10 (± 0.05) × 10^{15} molecules/cm^2, which was consistent with the formation of a dense monolayer (Yang et al., 2002; Zhong et al., 2007).

3.3. Feasibility study

Fluorescence-based nucleotide detection is the gold standard in conventional microarray analysis (Ekins et al., 1989; Fodor et al., 1991), and was therefore used as a proof-of-concept for our miRNA detection scheme shown in Fig. 1. For fluorescence-based miRNA detection, the same steps as depicted in Fig. 1 were used, except that a Cy3-conjugated SP was employed instead of a Au NP-conjugated SP. Figures 3A–D show the fluorescence images corresponding to decreasing concentrations of miR-208b target diluted in 5× SSC. Figure 3E represents the calibration curve whereby the fluorescence intensities obtained from the various arrays were plotted against the miR-208b target concentrations. The concentration range investigated was 1 pM–10 μM. The calibration curve displayed a linear range over 10 nM–100 nM, and the minimum detectable concentration was 1 pM, which was consistent with other reports (Zammatteo et al., 2000; Lehr et al., 2003; Livache et al., 2003). A direct visualization under fluorescence microscope demonstrated that the detection scheme was feasible for miRNA detection and quantification.

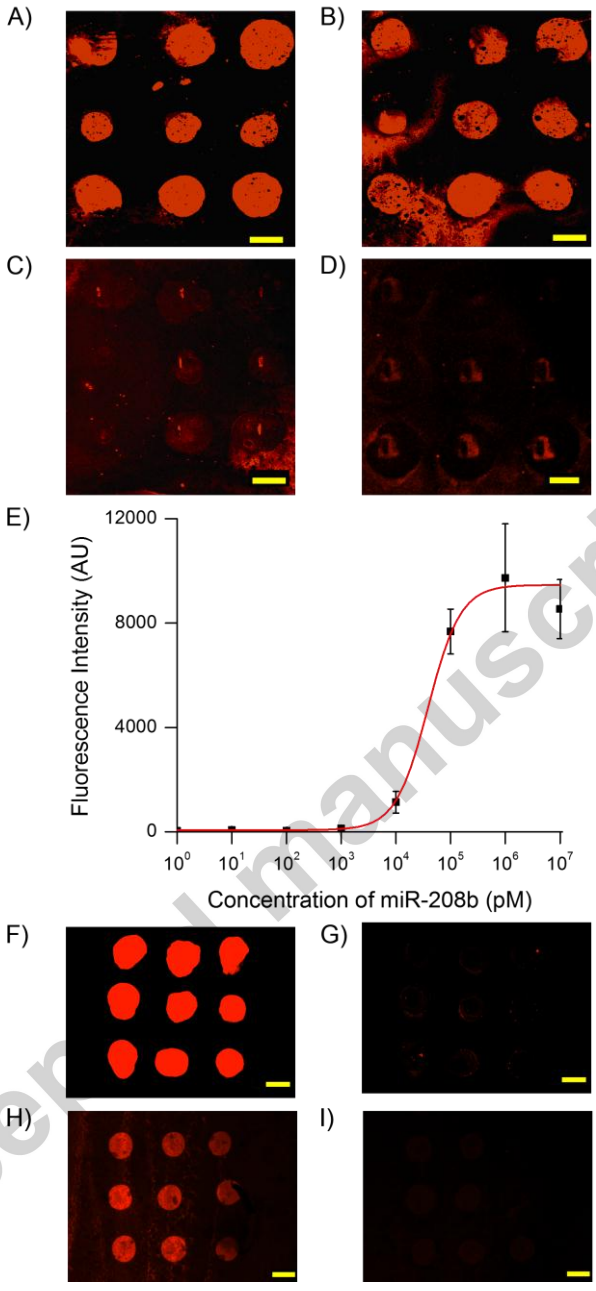

Fig. 3. Proof-of-concept demonstrated by fluorescence-based miRNA detection. Fluorescence images of on-chip hybridization between immobilized CPs and (A) 1 μM, (B) 10 nM, (C) 10 pM and (D) 100 fM of miR-208b targets. (E) Calibration curve for the fluorescence detection of miR-208b. Fluorescence images of Cy3-labeled SPs (F) immediately after spotting and (G) after stringent wash. Fluorescence images for the

hybridization of Cy3-labeled SPs to immobilized hairpin CPs (H) with prior target–CP hybridization and (I) without target. Scale bars = 100 μm.

A couple of issues, however, remained to be addressed, namely, non-specific adsorption of SPs onto the surface of glass slides, as well as SPs hybridizing with the stem region of hairpin CPs without the presence of the target. These phenomena would give rise to false-positive results, and render the detection assay inaccurate. To determine the amount of non-specific adsorption of SPs onto the microarray surface, we spotted 1 μM of Cy3-labeled SPs onto the carboxyl-PEG surface (Fig. 3F), followed by a stringent wash. The resulting fluorescence image showed only negligible fluorescence (Fig. 3G), indicating that there was almost no non-specific adsorption of Cy3-labeled SPs onto the carboxyl-PEG surface. The carboxyl layer would deprotonate at neutral pH (under SSC conditions), producing a negative charge that would repel nucleotide molecules, which are polyanions (Wu et al., 2011), hence reducing or eliminating non-specific adsorption of non-target nucleotide sequences.

To investigate if SPs would hybridize with the hairpin CPs even in the absence of target miRNAs, we immobilized hairpin CPs as described earlier. Next, 1 μM of Cy3-labeled SPs was applied to the immobilized hairpin CPs, and left to incubate at room temperature over 4 h. The glass slide was then washed and dried with nitrogen, and fluorescence image was taken. No or negligible fluorescence (Fig. 3I) was observed, as compared to an array added with 1 μM of perfect complementary target as positive control (Fig. 3H). Hence, we concluded that our surface functionalization and detection schemes were able to eliminate any non-specific adsorption and false-positive results, allowing our assay to be accurate and robust.

3.4. Detection of miRNA targets in buffer and biological fluids

Hairpin-structured CP was designed to capture miR-208b, which was chosen as our model miRNA. Plasma miR-208b levels can be used to detect patients with acute myocardial infarction (AMI), which would raise the circulating miR-208b in the plasma by 1600 folds (Corsten et al., 2010). Once the proof-of-concept was established with the fluorophore-labeled SPs, they were replaced by their Au NP-tagged counterparts. After

conducting the detection assay and hybridization steps described earlier, the amount of Au NPs was determined by DIC imaging. Fig. 4A–C represent the DIC images of Au NPs corresponding to different miR-208b concentrations in 5× SSC buffer. The DIC imaging technique was able to create a virtual 3D morphology of individual Au NPs, allowing simple visualization and quantification of miRNA targets in an unambiguous manner (Roy et al., 2011). For reference purpose, imaging of AuNP-tagged SPs on the microarray surface, used for the detection of miR-208b, was also done by FESEM (Supporting Information Fig. S1). The concentration range investigated was 10 fM–100 nM, and the limit of detection (LOD) was 10 fM (Fig. 4D), which was much lower as compared to that for fluorescence-based detection. In addition, the linear range was much wider (10 fM–100 nM).

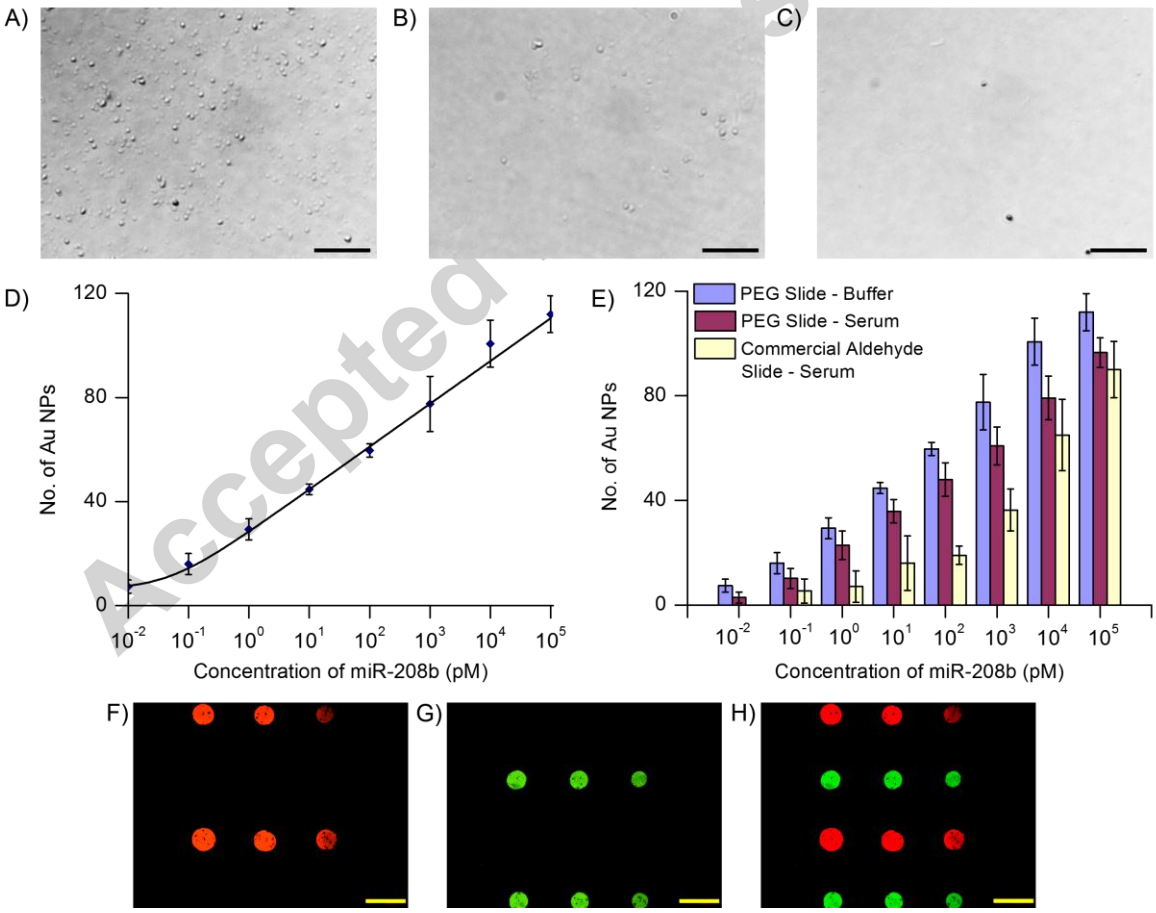

Fig. 4. Quantification of miRNAs via DIC imaging of Au NPs. Surface coverage of Au NPs corresponding to miR-208b target concentrations of (A) 1 nM, (B) 1 pM and (C) 1

fM, and (D) the associated calibration curve. Scale bars = 50 μm. (E) Comparison of miRNA target detection in buffer and human serum on carboxyl-PEG functionalized glass slides and commercial aldehyde glass slides. Multiplexed detection study showing the hybridization of a mix of (F) miR-208b and (G) miR-335 targets to their respective hairpin CPs, and (H) the overlaid image. Scale bars = 200 μm.

Since one of the principal objectives of this study was to minimize sample preparation steps and detect circulating miRNA targets directly from biological fluids, we made an attempt to detect the concentration of cardiac disease-specific miR-208b, which was spiked into commercially available human serum. Figure 4E compares the detection of miRNA target in 5× SSC buffer and in human serum on our carboxyl-PEG functionalized glass slide. A decrease in signal intensity of 22% (± 7%) for miRNA target detection in human serum was observed, as compared to that in buffer. However, a LOD of 10 fM was still achieved for miRNA target in human serum. Additionally, the linear range of 10 fM–100 nM was retained. The LOD of 10 fM was equivalent to ~ 6,000 copies of miRNA/μl of sample. As a reference, Mitchell *et al.* quantified specific miRNAs (miR-15b, miR-16, and miR-24) in plasma from healthy individuals using TaqMan quantitative RT-PCR (qRT-PCR) assays (Mitchell *et al.*, 2008). The concentration of the above miRNAs ranged from 9,000 to 134,000 copies/μl plasma, depending on the type of miRNA. Since the microarray developed in the present study offers a superior LOD, it is capable of handling low abundance miRNA in biofluids. Additionally, as the expression levels of many miRNAs are up-regulated, e.g. miR-208b and miR-499 are up-regulated by 1600 and 100 folds, respectively, for myocardial infarction (Corsten et al., 2010) and miR-223 is increased by 55 folds for metastatic prostate cancer (Watahiki et al., 2011), our microarray platform can potentially be used for disease diagnosis and screening. In some cases, however, subtle differences (≤ 10 folds) in the expression levels of circulating miRNAs may also be deterministic for disease diagnostics (Huang et al., 2010). To elucidate the resolution of our microarray, we examined if the differences in signal intensities for a given variation in the target miRNA concentration were statistically significant (Supporting Information Fig. S2). It was observed that the changes in output signal for every 10-fold increase of miR-208b

concentration in serum were statistically significant ($P < 0.05$). As such, our microarray was capable of detecting even a 10-fold change in expression level of circulating miRNAs, which were originally expressed at a concentration as low as 100 fM in human serum.

In general, differences in results between different studies and/or techniques could result from a couple of factors. (i) Expression of circulating miRNAs in serum may not correlate directly with those from tissues; the low concentrations of serum miRNAs may render them more relevant for up-regulation, and not down-regulation studies (Lodes et al., 2009). (ii) Different miRNA labeling and/or amplification techniques result in different miRNA expression profiles; amplification via RT-PCR result in different expression profiles compared to non-amplified samples (Lodes et al., 2009).

We have also compared the performance of our carboxyl-PEG coated microarray with commercial aldehyde glass slides, which do not possess an anti-fouling polymer layer (Fig. 4E). We chose the commercial aldehyde slides as a control as it is common for printing nucleic acid microarrays. Identical procedure was followed for both types of slides as described earlier. Using the commercial aldehyde glass slide, the LOD achieved (100 fM) was 1 order of magnitude inferior to our carboxyl-PEG slide, and signal intensities were generally much lower, especially at lower miRNA concentrations (100 fM–1 nM). Additionally, the linear range was reduced to ~ 100 pM–100 nM. Hence, our carboxyl-PEG coated microarray out-performed the commercial aldehyde slide in the detection of miRNA target in human serum. The protein-resistant property of PEG (Ko et al., 2001; Liu et al., 2004) has enabled our carboxyl-PEG microarray to sensitively detect target miRNA directly from biological fluids without extensive sample preparation steps.

To demonstrate the multiplexing capabilities of the microarray platform, 10 μM of hairpin CPs for miR-208b (1st and 3rd rows) and miR-335 (2nd and 4th rows) (Fig. 4F–H) were immobilized onto the carboxyl-PEG functionalized glass slide. Next, a solution containing 100 nM of Cy3-labeled miR-208b and 100 nM of FAM-labeled miR-335 targets was added to the array of CPs. Hybridization was allowed to occur at room temperature over 4 h, followed by stringent washes. The targets only hybridized to their respective CPs as Cy3 fluorescence was only seen on the 1st and 3rd rows and FAM fluorescence was only observed on the 2nd and 4th rows. Also, there was virtually no

cross-contamination even in the presence of a high concentration of non-complementary miRNAs, demonstrating that the immobilized CPs were very selective for their individual targets. The throughput could be easily scaled up for DIC imaging of Au NPs through spatial mapping of different CPs on the glass slide and software analysis of the images. This would allow for high-throughput miRNA quantification and profiling.

3.5. Discriminating sequence mismatches using hairpin and linear CPs

Members within a specific miRNA family often differ in sequence by only a single base. Hence, for an accurate analysis of miRNA expression profiles, it is important for detection assays to discriminate sequence mismatches with high accuracy. Additionally, many human diseases, such as cancer, occur due to point mutations in one or more genes (Sidransky, 2002), and such mutations can be used as important molecular markers to detect early-stage tumorigenesis (Diehl and Diaz, 2007). For our sequence mismatch discrimination study, we selected 4 members from the hsa-let-7 family, namely *let-7a*, *let-7b*, *let-7f* and *let-7g*, which have high sequence homology. Hairpin and linear CPs were designed in such a way that *let-7a* target was the perfect match (PM) for each of them. There was a single-base mismatch (1MM) between *let-7a* and *let-7f*, and a two-base mismatch (2MM) between *let-7a* and *let-7b*, as well as between *let-7a* and *let-7g* (Table 1). Figure 5 shows that when hairpin CP for *let-7a* was used, there is a ~ 74% drop in signal intensity for *let-7f* (1MM), and an even greater decrease (~ 80% and 84% respectively) for *let-7b* and *let-7g* (2MM), as compared to *let-7a* (PM). For *let-7b*, the two-base mismatch involves two A-T bonds, whereas that for *let-7g* involves one A-T and one C-G bond. Since a C-G pair is connected by three hydrogen bonds while an A-T pair involves two, the resulting decrease in melting temperature for base mismatch was greater for *let-7g* than for *let-7b*. Consequently, a greater decrease in signal intensity was observed for *let-7g* compared to *let-7b*, even though both targets contained two-base mismatch as compared to *let-7a*.

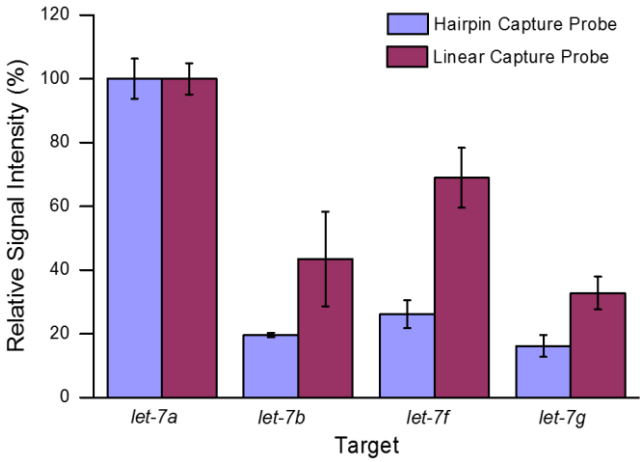

Fig. 5. Selectivity and sequence mismatch discrimination study among members of the *hsa-let-7* family, using hairpin and linear CPs for *let-7a*.

On the other hand, for a linear CP complementary to *let-7a*, we observed a smaller extent of decrease in signal intensities. There was a ~ 31% drop in signal intensity for *let-7f* (1MM), and a decrease of ~ 57% and 67%, respectively, for *let-7b* and *let-7g* (2MM), as compared to *let-7a* (PM). Due to their stem-loop structure, hairpin CPs are constrained molecules, therefore upon formation or dissociation of CP–target complex, they experience a greater structural reorganization as compared to linear CPs (Bonnet et al., 1999). This has enabled their increased sensitivity and ability to discriminate sequence mismatch. Furthermore, it has been reported that hairpin CPs demonstrate higher hybridization rates, and that hairpin CP–target complexes are more stable than their linear counterparts (Riccelli et al., 2001). These properties offer substantial advantages, especially in a POC setting, which requires rapid and sensitive signal readout for diagnostic purposes. A comparison of our microarray platform to other miRNA detection methods can be found in Supporting Information Table S1.

4. Conclusions

We have developed a microarray platform for highly sensitive and selective detection of disease-specific circulating miRNAs, with miR-208b as a model marker for cardiac disease. To our knowledge, this study is the first demonstration of a microarray-based technique that is capable of direct profiling of miRNA targets from human serum.

Our platform was able to detect as low as 10 fM (equivalent to ~ 6000 copies in a microliter sample) of target miRNAs in human serum, without the need for sample labeling or PCR amplification. Application of carboxyl-PEG functional layer on the microarray surface and exploitation of hairpin CPs enabled such outstanding performance. Our carboxyl-PEG functionalized microarray was superior to the commercial aldehyde slides in the detection of miRNA targets in human serum. This illustrated the importance of anti-fouling treatment for reducing interference from complex biological media. On a single microarray, we were also able to detect multiple targets with negligible cross-contamination, showing the potential for multiplexed assay. Furthermore, the microarray could discriminate between the members of a miRNA family with a high sequence homology. With all the aforementioned capabilities, our microarray platform might find potential application in the rapid and non-invasive profiling and quantification of circulating miRNAs in serum and plasma samples for POC diagnostic purposes.

Acknowledgements

This work was funded by the Institute of Bioengineering and Nanotechnology (Biomedical Research Council, Agency for Science, Technology and Research, Singapore).

References

Ambros, V., 2004. Nature, 431, 350-355.

Bartel, D. P., 2004. Cell, 116, 281-297.

Bonnet, G., Tyagi, S., Libchaber, A., Kramer, F. R., 1999. Proc. Natl. Acad. Sci. U.S.A., 96, 6171-6176.

Calin, G. A., Croce, C. M., 2006. Nat. Rev. Cancer, 6, 857-866.

Chen, X., Ba, Y., Ma, L., Cai, X., Yin, Y., Wang, K., Guo, J., Zhang, Y., Chen, J., Guo, X., Li, Q., Li, X., Wang, W., Wang, J., Jiang, X., Xiang, Y., Xu, C., Zheng, P., Zhang, J., Li, R., Zhang, H., Shang, X., Gong, T., Ning, G., Zen, K., Zhang, C. Y., 2008. Cell Res., 18, 997-1006.

Chim, S. S. C., Shing, T. K. F., Hung, E. C. W., Leung, T.-y., Lau, T.-k., Chiu, R. W. K., Lo, Y. M. D., 2008. Clin. Chem., 54, 482-490.

Corsten, M. F., Dennert, R., Jochems, S., Kuznetsova, T., Devaux, Y., Hofstra, L., Wagner, D. R., Staessen, J. A., Heymans, S., Schroen, B., 2010. Circ. Cardiovasc. Genet., 3, 499-506.

De, M., Rana, S., Akpinar, H., Miranda, O. R., Arvizo, R. R., Bunz, U. H. F., Rotello, V. M., 2009. Nat. Chem., 1, 461-465.

Diehl, F., Diaz, L. A. J., 2007. Curr. Opin. Oncol., 19, 36-42.

Ekins, R., Chu, F., Biggart, E., 1989. Anal. Chim. Acta, 227, 73-96.

Esquela-Kerscher, A., Slack, F. J., 2006. Nat. Rev. Cancer, 6, 259-269.

Fodor, S. P., Read, J. L., Pirrung, M. C., Stryer, L., Lu, A. T., Solas, D., 1991. Science, 251, 767-773.

Gilad, S., Meiri, E., Yogev, Y., Benjamin, S., Lebanony, D., Yerushalmi, N., Benjamin, H., Kushnir, M., Cholakh, H., Melamed, N., Bentwich, Z., Hod, M., Goren, Y., Chajut, A., 2008. PLoS One, 3, e3148-e3154.

Halliwell, C. M., Cass, A. E., 2001. Anal. Chem., 73, 2476-2483.

Hanke, M., Hoefig, K., Merz, H., Feller, A. C., Kausch, I., Jocham, D., Warnecke, J. M., Sczakiel, G., 2010. Urol. Oncol., 28, 655-661.

Heneghan, H. M., Miller, N., Kerin, M. J., 2010. J. Clin. Oncol., 28, e573-574.

Hou, J., Zhang, H., Yang, Q., Li, M., Jiang, L., Song, Y., 2015. Small, 11, 2738-2742.

Hou, J., Zhang, H. C., Yang, Q., Li, M. Z., Song, Y. L., Jiang, L., 2014. Angew Chem Int Edit, 53, 5791-5795.

Huang, Z., Huang, D., Ni, S., Peng, Z., Sheng, W., Du, X., 2010. Int. J. Cancer, 127, 118-126.

Kloosterman, W. P., Plasterk, R. H., 2006. Dev. Cell, 11, 441-450.

Ko, Y. G., Kim, Y. H., Park, K. D., Lee, H. J., Lee, W. K., Park, H. D., Kim, S. H., Lee, G. S., Ahn, D. J., 2001. Biomaterials, 22, 2115-2123.

Lehr, H. P., Reimann, M., Brandenburg, A., Sulz, G., Klapproth, H., 2003. Anal. Chem., 75, 2414-2420.

Lewis, E. K., Haaland, W. C., Nguyen, F., Heller, D. A., Allen, M. J., MacGregor, R. R., Berger, C. S., Willingham, B., Burns, L. A., Scott, G. B., Kittrell, C., Johnson, B. R., Curl, R. F., Metzker, M. L., 2005. Proc. Natl. Acad. Sci. U.S.A., 102, 5346-5351.

Liu, J., Pan, T., Woolley, A. T., Lee, M. L., 2004. Anal. Chem., 76, 6948-6955.

Livache, T., Maillart, E., Lassalle, N., Mailley, P., Corso, B., Guedon, P., Roget, A., Levy, Y., 2003. J. Pharm. Biomed. Anal., 32, 687-696.

Lodes, M. J., Caraballo, M., Suciu, D., Munro, S., Kumar, A., Anderson, B., 2009. PLoS One, 4, e6229.

Mitchell, P. S., Parkin, R. K., Kroh, E. M., Fritz, B. R., Wyman, S. K., Pogosova-Agadjanyan, E. L., Peterson, A., Noteboom, J., O'Briant, K. C., Allen, A., Lin, D. W., Urban, N., Drescher, C. W., Knudsen, B. S., Stirewalt, D. L., Gentleman, R., Vessella, R. L., Nelson, P. S., Martin, D. B., Tewari, M., 2008. Proc. Natl. Acad. Sci. U.S.A., 105, 10513-10518.

Oh, S. J., Ju, J., Kim, B. C., Ko, E., Hong, B. J., Park, J.-G., Park, J. W., Choi, K. Y., 2005. Nucleic Acids Res., 33, e90-e97.

Riccelli, P. V., Merante, F., Leung, K. T., Bortolin, S., Zastawny, R. L., Janeczko, R., Benight, A. S., 2001. Nucleic Acids Res., 29, 996-1004.

Rodiger, S., Ruhland, M., Schmidt, C., Schroder, C., Grossmann, K., Bohm, A., Nitschke, J., Berger, I., Schimke, I., Schierack, P., 2011. Anal. Chem., 83, 3379-3385.

Roy, S., Chen, X., Li, M. H., Peng, Y., Anariba, F., Gao, Z., 2009. J. Am. Chem. Soc., 131, 12211-12217.

Roy, S., Soh, J. H., Gao, Z., 2011. Lab Chip, 11, 1886-1894.

Sano, S., Kato, K., Ikada, Y., 1993. Biomaterials, 14, 817-822.

Sidransky, D., 2002. Nat. Rev. Cancer, 2, 210-219.

Stefani, G., Slack, F. J., 2008. Nat. Rev. Mol. Cell Biol., 9, 219-230.

Stern, E., Vacic, A., Rajan, N. K., Criscione, J. M., Park, J., Ilic, B. R., Mooney, D. J., Reed, M. A., Fahmy, T. M., 2010. Nat. Nanotechnol., 5, 138-142.

Tiraferri, A., Elimelech, M., 2012. J. Membrane Sci., 389, 499-508.

Tyagi, S., Bratu, D. P., Kramer, F. R., 1998. Nat. Biotechnol., 16, 49-53.

Wang, G., Tam, L. S., Li, E. K., Kwan, B. C., Chow, K. M., Luk, C. C., Li, P. K., Szeto, C. C., 2010. J. Rheumatol., 37, 2516-2522.

Watahiki, A., Wang, Y., Morris, J., Dennis, K., O'Dwyer, H. M., Gleave, M., Gout, P. W., 2011. PLoS One, 6, e24950.

Weber, J. A., Baxter, D. H., Zhang, S., Huang, D. Y., Huang, K. H., Lee, M. J., Galas, D. J., Wang, K., 2010. Clin. Chem., 56, 1733-1741.

Wu, M., Kempaiah, R., Huang, P. J., Maheshwari, V., Liu, J., 2011. Langmuir, 27, 2731-2738.

Yang, W., Auciello, O., Butler, J. E., Cai, W., Carlisle, J. A., Gerbi, J. E., Gruen, D. M., Knickerbocker, T., Lasseter, T. L., Russell, J. N., Jr., Smith, L. M., Hamers, R. J., 2002. Nat. Mater., 1, 253-257.

Zammatteo, N., Jeanmart, L., Hamels, S., Courtois, S., Louette, P., Hevesi, L., Remacle, J., 2000. Anal. Biochem., 280, 143-150.

Zampetaki, A., Kiechl, S., Drozdov, I., Willeit, P., Mayr, U., Prokopi, M., Mayr, A., Weger, S., Oberhollenzer, F., Bonora, E., Shah, A., Willeit, J., Mayr, M., 2010. Circ. Res., 107, 810-817.

Zhang, Y., Diao, Z., Su, L., Sun, H., Li, R., Cui, H., Hu, Y., 2009. AJOG, 202, e1-7.

Zhao, H., Shen, J., Medico, L., Wang, D., Ambrosone, C. B., Liu, S., 2010. PLoS One, 5, e13735-e13746.

Zhong, Y. L., Chong, K. F., May, P. W., Chen, Z. K., Loh, K. P., 2007. Langmuir, 23, 5824-5830.

Zu, Y., Gao, Z., 2009. Anal. Chem., 81, 8523-8528.

Highlights

- A label-free and highly sensitive glass slide-based microarray for the detection of micro-RNAs (miRNAs) in human serum is developed.
- Surface functionalization of a carboxyl-PEG layer on the glass slide minimizes non-specific binding of biomolecules and provides anti-fouling effect, allowing direct detection of 10 fM of miRNA targets in 20 µl of unprocessed human serum.
- Specific hairpin-structured capture probes were designed, enabling increased detection sensitivity and the ability to discriminate single-base mismatches.

- Differential interference contrast (DIC) microscopy provides a facile and direct method for the visualization of gold nanoparticle signaling probes using an optical microscope.
- Furthermore, the microarray is able to detect multiple targets with negligible cross-contamination in a multiplexed assay.